Scientific Research Publishing

Open Journal of Applied Sciences, 2025, 15(10), 3025-3042
https://www.scirp.org/journal/ojapps
ISSN Online: 2165-3925
ISSN Print: 2165-3917

Multifractal Detrended Fluctuation Analysis of Solar Wind Speed and Interplanetary Magnetic Field during Solar Cycle 24

Adébiyi Joseph Adéchinan[1], Tokpanoudé D. Judicaël[2], Kpomahou Y. J. Fernando[3]

[1]Department of Physics, Faculty of Science and Technology of Natitingou, National University of Science, Technology, Engineering and Mathematics (UNSTIM), Natitingou, Benin
[2]Doctoral School of Sciences, Technologies, Engineering and Mathematics, University of Science, Technology, Engineering and Mathematics (UNSTIM), Abomey, Benin
[3]National School of Higher Technical Education of Lokossa, University of Science, Technology, Engineering and Mathematics (UNSTIM), Lokossa, Benin
Email: adechinan.joseph@unstim.bj

How to cite this paper: Adéchinan, A.J., Judicaël, T.D. and Fernando, K.Y.J. (2025) Multifractal Detrended Fluctuation Analysis of Solar Wind Speed and Interplanetary Magnetic Field during Solar Cycle 24. *Open Journal of Applied Sciences*, **15**, 3025-3042.
https://doi.org/10.4236/ojapps.2025.1510199

Received: September 1, 2025
Accepted: October 8, 2025
Published: October 11, 2025

Abstract

This paper investigates the nature of the fluctuation of both solar wind speed and the interplanetary magnetic field intensity during solar cycle 24. Since detrended multifractal fluctuation analysis can provide information about the internal regularity, randomness, and long-term correlation of time series, we applied this technique to our two time series data to better understand their evolution regularity and analyze their multifractal behavior. The results indicate the existence of strong multifractal characteristics in both data sets studied. According to the width of the multifractal spectra of the two series, the solar wind speed exhibits a more complex multifractal behavior than the interplanetary magnetic field. The different parameters from the multifractal spectra show that this multifractality is dependent on both a fat-tailed probability density function and long-range temporal correlations. Furthermore, the multifractality identified in both time series appears to be associated with an energy cascade process.

Keywords

Wind Speed, Magnetic Field, Fluctuation, MFDFA, Solar Cycle 24

1. Introduction

The Sun-Earth system is a complex system, composed of multiple interactions. These interactions result in energy transfers from regions of the Sun to the near

Earth space environment [1]. This energy is primarily transported by a stream of particles called the solar wind. It is therefore a low-density plasma, made up of charged particles in particular, electrons, ions and protons [1]-[3]. With a speed generally between 300 and 800 km/s depending on the origin, it plays a fundamental role in the dynamics of the interplanetary medium and Sun-Earth interactions. This solar wind then interacts with the Earth's magnetosphere.

These interactions between the solar wind and the magnetosphere are thus complex phenomena because of the magnetic reconnection which induces exchanges of plasma and energy between the two [3]. During this process, there is sometimes a simultaneous release of large quantities of magnetized plasma, known as a Coronal Mass Ejection (CME). When the CME subsequently interacts with the Earth's magnetic field, it induces disturbances that can have a significant impact on critical infrastructure [2]-[4]. Scientific opinion now converges on the fact that coronal mass ejections are the cause of most disturbances on the ground, more than solar flares, which are accidental [5]. Moreover, the interplanetary magnetic field results from the extension of the solar magnetic field and its transport by the solar wind. Like the solar wind, it is an important factor in modulating the near-Earth space environment. The orientation of this field is very important for the magnetosphere ionosphere coupling, since it determines the efficiency of magnetic reconnection at the magnetopause [6]-[9].

Several studies have shown that variations in the solar wind speed are not only linked to the structure of the solar magnetic field but also to the evolution of the solar cycle, and they condition the nature of the couplings with the Earth's magnetosphere [3]-[5] [10]-[13]. Indeed, the dynamics of the Sun has a cyclical component called the solar cycle. It is the period at the end of which solar activity varies, reproducing the same phenomena as during the previous period of the same duration. The solar cycle lasts approximately eleven years and is measured in particular by observing the number and location of sunspots, which constitute the most obvious manifestation of solar activity [5] [7] [9]. The effects of the space radiation environment on human activities are strongly linked to solar activity and geomagnetic activity. These permanently disrupt the radiative balance of the regions crossed by satellite orbits. The consequences of the space radiation environment are multiple and diverse. They can impact aerospace infrastructure by causing irreversible damage. Sun-Earth interactions can also disrupt terrestrial telecommunications, satellite positioning systems, and aeronautical systems, potentially endangering aircraft and their passengers. Furthermore, consequences on Earth can even be observed through geomagnetically induced currents, which can, for example, damage transformers and high-voltage lines. Lanzerotti *et al.* [14] even add biological effects to this list. In view of these possible damages, it is becoming increasingly important to be able to predict the dynamics of geomagnetic activity.

Numerous studies exist in the literature on the solar wind, its speed and the interplanetary magnetic field. These investigations show that these two phenom-

ena have a non-stationary character [1]-[4] [6] [12]-[14]. Indeed, most natural phenomena often present self-similar structures and fluctuations at different scales [15]. To better understand these fluctuations in depth, the use of simple ordinary tools such as linear correlations is not appropriate because of the non-linear nature of these variables. Fortunately, several tools are now being developed for such processes. Among these, the most common is Multifractal Detrended Fluctuation Analysis (MFDFA). This approach is applied in several fields, including physics [1]-[6] [11]-[16], finance [17]-[20], and environmental sciences [21]-[33]. The important advantage of MFDFA over other approaches is its ability to detect long-term correlations in non-stationary time series. Multifractal analysis proves to be a powerful tool for characterizing the complexity and heterogeneity of fluctuations in natural phenomena because it allows describing the distribution of local singularities in a time or spatial series and identifying the different scales of intermittency and self-organization in the dynamics of a physical or geophysical signal. Thus, the study of the multifractal characteristics of natural phenomena is an essential research topic for understanding the complex dynamics of physical and geophysical systems.

Gomes *et al.* [1] used a multifractal relaxed fluctuation analysis coupled with surrogate and volatility methods to study the effects of current sheets on solar wind turbulence. Starting from a p-model to reproduce the multifractal behavior of the solar wind series, they found that a nonlinear turbulence energy cascade dynamic system is at the origin of the dynamics observed in the data series they used. Macek *et al.* [2] investigated the intermittency and multifractality of the solar wind using both magnetic field data collected by Voyager in the outer heliosphere and plasma data recorded by Helios in the inner heliosphere. They showed that the multifractal spectrum of the solar wind attractor is consistent with that of the multifractal measure of the self-similar weighted Baker map. Salam *et al.* [3] used wavelet transforms to study the scaling and intermittency properties of solar wind MHD turbulence. They obtained results similar to those previously reported by other authors [4]-[6]. According to these authors, the scaling of the magnetic field and the velocity fluctuations are found to be fundamentally different. Indeed, the magnetic field and the bulk plasma velocity have fundamentally different scaling laws, close to K41 for the magnetic field components, and close to IK for the velocity components. Bolzan *et al.* [7] analyzed the interplanetary magnetic field obtained by the ACE satellite during coronal mass ejections. Their multifractal analysis showed that the presence of these strong and well-behaved structures in the coronal mass ejection decreases the degree of multifractality, compared to periods following the ejections. This trend was also found by Li *et al.* [8], who also observed this behavior on geomagnetic time series where, according to them, the presence of strong oscillations strongly reduces the degree of multifractality of the signal.

The main objective of this work is to use the MFDFA method to characterize and compare the complexity of fluctuation dynamic both of the solar wind speed

and the interplanetary magnetic field during solar cycle 24. This paper is organized as follows: the first part of Section 2 presents the data used in the study. The second part of Section 2 details the methodology adopted, *i.e.*, the different steps to follow to apply the MFDFA method to a time series of data. Section 3 presents the main results of the study as well as their analysis and interpretation. Finally, some conclusions and future work are provided in Section 4.

2. Data and Methodology

2.1. Data

Understanding the Sun-Earth interaction involves observing and analyzing the solar wind. In our study, we focused on using the OMNIweb database. OMNIweb is a NASA online service that provides data on the space environment around Earth. that offers a comprehensive history of solar wind parameters, bringing together measurements made by various successive missions. These data contribute to a better understanding of the impact of solar activity on Earth's atmosphere and weather. The vast collection of historical solar wind data and the regular updates to this dataset make OMNI a valuable asset for understanding the past and present of the Earth-Sun relationship. The information stored on the omminweb site comes mainly from orbiting satellites and space probes such as: ACE, WIND, DSCOVR, IMP-8, etc. These different satellites measure, among other things, in real time certain intrinsic characteristics (speed, density, temperature) of the solar wind, the components of the interplanetary magnetic field, geomagnetic parameters (Kp, Dst, AE indices, etc.), as well as solar flares and energetic particles. Furthermore, a technological effort is being made to intercalibrate these data and project them onto the shock wave nose to ensure spatial consistency.

The data available on the OMNIweb site are provided at two time scales. These are low-frequency data (with a recording scale of one hour) and high-frequency data (with a recording scale of the order of minutes). For this study, we used both solar wind speed data and mean magnetic field strength in the interplanetary medium, collected with a one-minute resolution during solar cycle 24, ranging from December 2008 to December 2019. Despite the presence of time holes gaps in some data time series due for example to a momentary failure of an instrument, the solar wind parameters made available on OMNIweb are well suited for use in data-driven models. Indeed, these time holes, when they are not too large, can be filled using different interpolation techniques. It is important to point out that in the specific case of our work, the data used is complete. Thus, we did not use any interpolation technique.

2.2. Methodology

According to several authors, detrended multifractal fluctuation analysis is a powerful tool for identifying scaling behaviors and multifractal properties of non-stationary time series. It is based on eliminating the intrinsic fluctuation of the signal from the time series, by distinguishing the polynomial trends of the signal. This

technique was initially developed by Peng *et al.* [31], as basic Detrended Fluctutation Analysis (DFA) and later extended to the study of multifractal processes by Kandelhardt *et al.* [32], under the name MFDFA. The MFDFA method is in other words, the modified version of the generalized detrended fluctuation analysis. The detailed computational procedure can be found as follows [6]-[10] [14] [16]-[20] [30]. Consider any given time series $x(i)$ containing N discrete data ($i=1,2,\cdots,N$), the steps to apply the MFDFA method to this series are as follows:

Step 1: The first step in this method is to create a cumulative sum of the original time series x_k. The profile Y_i is created by converting the noises into random walks. The objective of this transformation is to align the analysis with stationary assumptions. This therefore allows a more precise exploration of intrinsic fractal characteristics while removing superficial trends. The accumulated deviation of the series can be calculated as using Equation (1)

$$Y(i)=\sum_{i}^{k}\left(x_i-\overline{x}\right), \tag{1}$$

where $\overline{x}$ is the mean of the original series.

Step 2: The second step is to divide the integrated series $Y(i)$ into non-overlapping intervals by the equal length s. There are $N_s=int(N/s)$ segments and N_s is the nearest integer part of N/s. Since the length N of the series may not be an integer multiple of the timescale s, some data may remain at the end of the series $Y(i)$. In order not to ignore the rest of the series, the same computation procedure is repeated from the end to the start of the series. Finaly, $2N_s$ segments are obtained in total. Such double segmentation tends to minimize the boundary effects and ensure sufficient stability. In each segment, a local trend is fitted using a polynomial of degree m.

Step 3: A least squares fit method is applied to calculate the trend for all of the $2N_s$ segments, and the variance is determined by:

$$F^2(s,\nu)=\begin{cases}\dfrac{1}{s}\displaystyle\sum_{i=1}^{s}\left[Y\left((\nu-1)s+i\right)-y_{\nu}^{(m)}(i)\right]^2, \nu=1,2,\cdots,N_s\\ \dfrac{1}{s}\displaystyle\sum_{i=1}^{s}\left[Y\left(N-(\nu-1)s+i\right)-y_{\nu}^{(m)}(i)\right]^2, \nu=N_s+1,\cdots,2N_s\end{cases} \tag{2}$$

The order of the polynomial $y_{\nu}^{(m)}(i)$ determines the order of trend in the time series which will be removed. For the linear (*i.e.*, polynomial order $m=1$), quadratic (*i.e.*, $m=2$), cubic (*i.e.*, $m=3$) or higher order polynomials, MFDFAm are denoted accordingly like MFDFA1, MFDFA2, MFDFA3 and so on [11].

Step 4: In MFDFAm, possible m order trends are eliminated in the profile. By averaging over all windows, we obtain the fluctuation as

$$F_q(s)=\left[\frac{1}{2N_s}\sum_{\nu=1}^{2N_s}\left(F^2(s,\nu)\right)^{\frac{q}{2}}\right]^{\frac{1}{q}} \tag{3}$$

where q is the order of moment. It is the fluctuation parameter which can be any real value except zero. Indeed when q tends towards zero, $F_q(s)$ will diverge. So

a logarithmic average has been taken to find $F_q(s)$ at q tends towards zero as:

$$F_0(s) = \exp\left[\frac{1}{4N_s}\sum_{\nu=1}^{2N_s}\ln\left(\left|F^2(s,\nu)\right|\right)\right] \tag{4}$$

This procedure is repeated for different scale length s and $F_q(s)$ for different values of q is computed.

Step 5: The final step is to estimate the slope of the log-log plot of $F_q(s)$ versus s for each value of q. From this plot, the scaling behaviour of the fluctuation functions can be determined. If the series $X(i)$ are long-range power-law correlated, $F_q(s)$ increases with increase of s, as a power-law

$$F_q(s) \sim s^{h(q)} \tag{5}$$

where $h(q)$ is the slope in a log-log plot of $F_q(s)$ versus s called the generalized Hurst exponent, which characterizes the fractal properties of the time series. Form the log-log plot of $F_q(s)$ against s, $h(q)$ is computed for various values of q. The moment q can take values between $-\infty$ and $+\infty$. For positive values of q, $h(q)$ describes the scaling behavior of segments with large uctuations and for negative values of q, $h(q)$ describes the scaling behavior of segments with small uctuations. If $h(q)$ varies with q, we deduce that the scale is multifractal. According to Kantelhardt *et al.* [32], this dependence is one of the intrinsic characteristics of a multifractal process. But to avoid a divergence of the moments the fat tails of the fluctuation distribution, several authors suggest restricting the order q [33]-[36]. In our paper, the moment q from −5 to +5 with the increment of 1. This choice of parameters follows several tests. On the other hand, if $h(q)$ does not depend on q and keeps a constant value H whatever q, then we conclude that the time series is monofractal. H is known as the Hurst exponent and represents an important parameter in the analysis of fractal and chaotic time series, since it allows to quantify the degree of persistence, long-term memory or randomness of a time series. This parameter, which varies between 0 and 1, therefore characterizes the degree to which past values of a chronological series can influence future values. If $H = 0.5$ the process is memoryless. There is no correlation and the time series is an uncorrelated signal (white noise). $H > 0.5$ implies long-term persistence and $H < 0.5$ implies short-term persistence.

It is important to note that when the time series is multifractal, the generalized Hurst exponent $h(q)$ is in turn related to the multifractal exponent also called Rènyi exponent $\tau(q)$ through the following formular. If the curve representing the evolution of $\tau(q)$ as a function of q is linear, then the time series is monofractal. On the other hand, if it is non-linear, then the time series has multifractal properties.

$$\tau(q) = qh(q) - 1, \tag{6}$$

On the basis of the obtained $\tau(q)$ characteristic, it is possible to get more information about the data series and properly characterize the strength of multifractality by calculating the Holder exponents α and the singularity spectrum

$f(\alpha)$ witch is an important tool in fractal investigation for the time series. These functions obtained by a first-order legend transformation are given by:

$$\begin{cases} \alpha(q) = \tau'(q) \\ f(\alpha) = q\alpha - \tau(q) \end{cases} \tag{7}$$

Figure 1 is a schematic representation of a singularity spectrum. From this figure, a set of parameters allowing each series to be characterized can be obtained. These are:

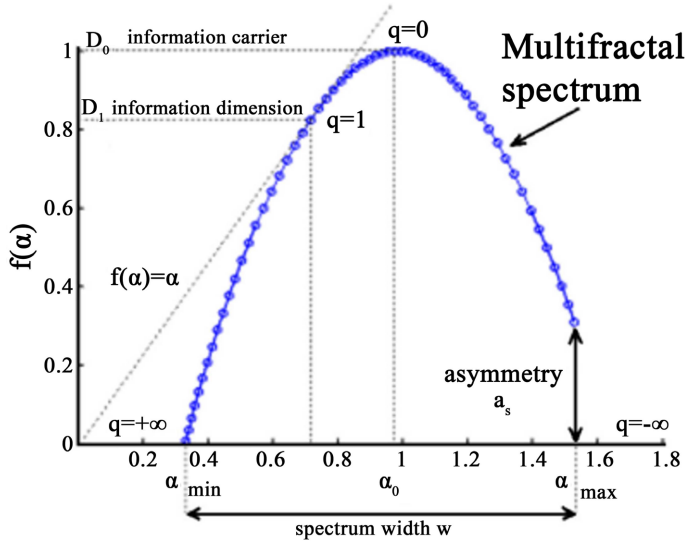

Figure 1. Example of a schematic representation of any multifractal spectrum including some important intrinsic parameters [13].

1) α_0, the α value when $f(\alpha)$ reaches its maximum value. It is obtained by setting $f(\alpha)=1$. Generally, the underlying process is more regular in appearance for low values of α.;

2) W, the α width

$$W = \alpha_{\max} - \alpha_{\min} \tag{8}$$

where $\alpha_{\max}$ and $\alpha_{\min}$ are respectively the minimum and maximum values of α that mark the base of the concave parable in the multifractal spectrum. $\alpha_{\max}$ and $\alpha_{\min}$ are obtained by setting $f(\alpha)=0$. According to several authors, the width of the spectrum w can be considered as a real indicator of the degree or complexity of the multifractality of the series studied. A large width indicates that the probability distribution is more heterogeneous and the time series has strong multifractality. On the contrary, a small width indicates that the fractal region is more uniformly distributed.

3) a_s, the asymmetry parameter

$$a_s = \frac{\alpha_{\max} - \alpha_0}{\alpha_0 - \alpha_{\min}} \tag{9}$$

the spectrum is symmetric if $a_s = 1$, for $a_s > 1$, the spectrum is right-skewed and

for $a_s < 1$, the spectrum is left-skewed [17] [20]. A multifractal spectrum with a long right tail has a greater contribution from small fluctuations. In contrast, a multifractal spectrum with left asymmetry has a greater influence from local fluctuations with large values [4].

Furthermore, Δf is an additional parameter that can be deduced from the multifractal spectrum. It is defined by:

$$\Delta f = f\left(\alpha_{\max}\right) - f\left(\alpha_{\min}\right) \tag{10}$$

For positive values of f, the number of largest subsets is greater than the minimum number in the probability measures and thus the multiscale fractal spectrum has the left hook shape. In contrast, For negative values of f, the multiscale fractal spectrum is right hook shape.

Furthermore, it is possible to identify the origin of multifractality in a given time series. In the literature, there are two possible sources: the shuffling procedure and the surrogating procedure [37]. On the one hand, multifractality due to a broad probability density function for the values of the time series; and on the other hand, multifractality due to different long-term correlations of small and large fluctuations. Indeed, we can determine the source of multifractality by analyzing the corresponding random series. The technique is to place the values in a random order during the shuffling procedure. This destroys all correlations. Thus, if the multifractality is due to long-range correlations, the shuffled series presents a non-fractal scaling. On the other hand, if the initial $h(q)$ dependence does not change, then the multifractality is due to the broad probability density, which is not affected by the shuffling procedure [38]. It is also important to note that when both sources of multifractality are present in the data series studied, the shuffled series will present a weaker multifractality than the initial series. To obtain the surrogate data in our case, we used the usual amplitude-adjusted Fourier transform method. According to Dong *et al.* [39], this technique consists to: 1) performing a discrete Fourier transform of the original series, 2) multiplying the discrete Fourier transform of the data by random phases, and 3) generating a phase randomized surrogate by performing an inverse Fourier transform.

In our study, the different steps of the MFDFA method that we have just described were applied to both the solar wind speed data and the interplanetary magnetic field intensity data recorded during solar cycle 24. The main results obtained at the end of this procedure are presented in the following section.

3. Results

3.1. Solar Wind Speed

Figure 2 shows the temporal variation of the strength of the solar wind during the study period. As can be seen in this figure, the speed of the solar wind varies greatly during solar cycle 24. It can take values ranging from 230.5 to 944 km/h with an average of 418.4 km/h. The solar cycle therefore recorded both slow solar winds (speeds below 400 km/h) and fast solar winds (speeds between 400 km/h

and 800 km/h). These values are perfectly in agreement with those found in several works [15] [27] [33].

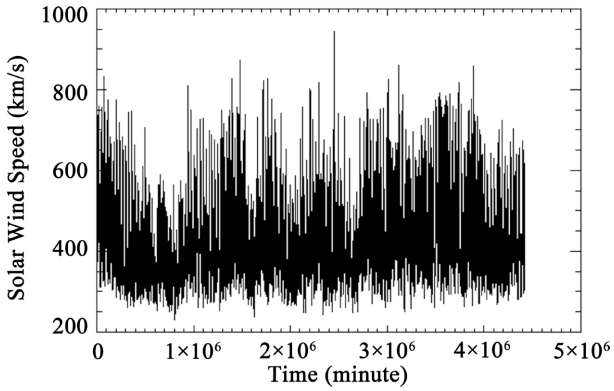

Figure 2. Variation of solar wind speed time series during solar cycle 24.

As we pointed out above, in MFDFA any kind of detrending is retained in the profile. In **Figure 3(a)**, the fluctuation spectrum $F(s)$ is plotted against s in a log-log diagram for the specific case where $q = 2$. Overall, the observed trend is the same for all values of order m. The fluctuation spectrum increases as the length of the segments increases. On the other hand, the fluctuations decrease when the order of the polynomial increases. **Figure 3(b)** shows the generalized Hurst exponents $h(q)$ against q. The chosen values of q varying between −5 and 5 with a step equal to 1. As can be seen from this figure, a general trend emerges. The generalized Hurst exponent is not independent of the moment q. Indeed, $h(q)$ decreases with increasing moment q regardless of the order of the polynomial. This variation of $h(q)$ as a function of q suggests the existence of multifractal behavior in the solar wind speed series during solar cycle 24. Furthermore, it is noted that the values of the Hölder exponent α are greater than 0.5. This observation indicates that both small and large fluctuations exhibit long-term persistent properties in this time series.

As we mentioned in the previous sections, to better quantify the multifractality of a given system, it is generally recommended to carefully analyze the representative curve of the singularity spectrum $f(\alpha)$ as a function of a singularity strength α. This function therefore makes it possible to describe the singularities that appear in the probability measure attributed to different regions of the phase space of a given dynamical system [10]. Compared to other variables, the multifractal singularity spectrum is easier to interpret theoretically by comparing experimental results with the studied models. To do this, we therefore represented in **Figure 3(c)**, the multifractal spectrum $f(\alpha)$ of solar wind speed occur during solar cycle 24. We note that the curve obtained has the appearance of a concave function of α. This form of the function $f(\alpha)$ has a universal character in multifractal theory [1] [3] [5]-[7]. The multifractal spectrum can either be left or right truncated. In our case, the asymmetry parameter obtained is positive and

greater than 1 ($a_s = 2.31$). So we have a right truncated multifractal spectrum for all values m of the order of the polynomial, indicates that the time series is insensitive to local fluctuations with small magnitudes. In other words, this shape of the multifractal spectrum allows us to say that the scaling behavior of the solar wind speed during solar cycle 24 is dominated by periods with stronger fluctuations. The dynamics of the solar wind is mainly marked by fast winds which are characterized by high speeds. The variability therefore comes from intense episodes. The width of this curve is an additional parameter witch can be identified as the degree of multifractality. In Figure 3(c), this width is large, which means that the probability distribution is more heterogeneous and therefore the degree of multifractality of the solar wind speed fields is high. Since the types of sources for multifractality in our time series could be different temporal correlations for small and large fluctuations or a fat-tailed probability distribution for the values of the time series, we then computed the corresponding multifractal spectrum width for the original series, shued series, and surrogated series. This allows us to concretely evaluate the multifractality contributions of these two types of sources.

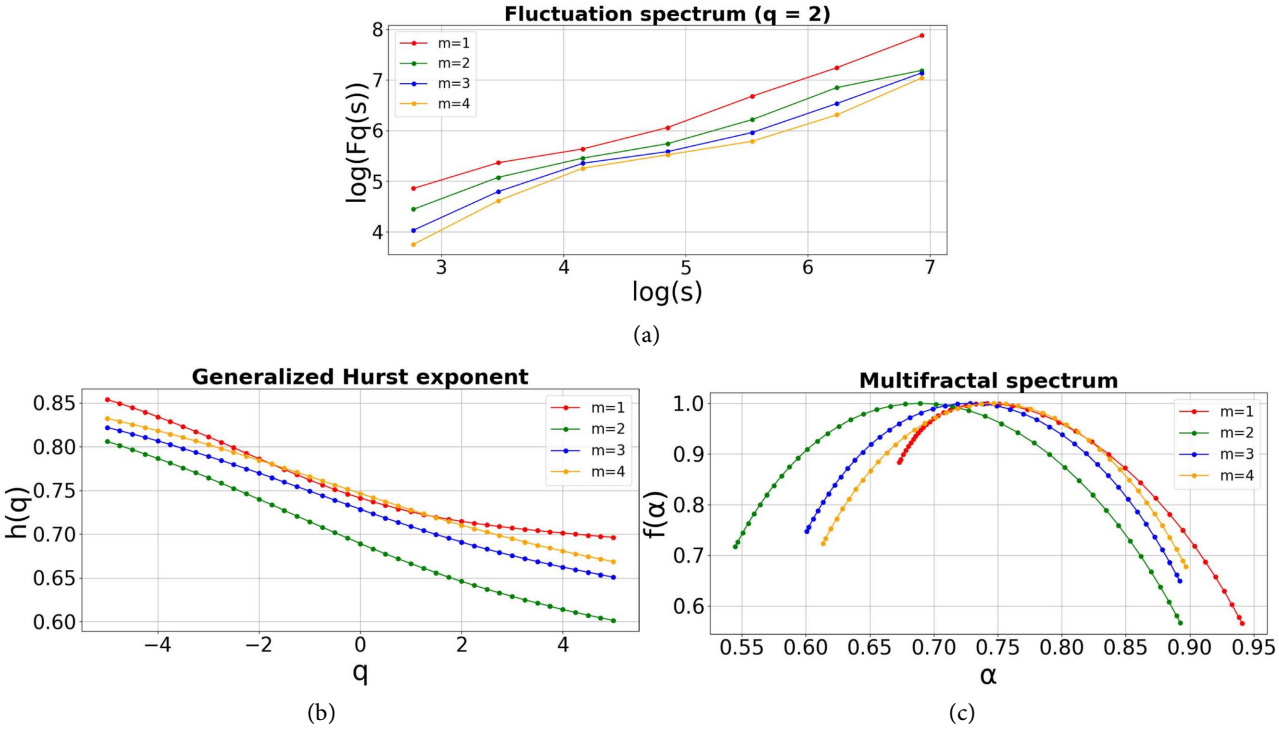

Figure 3. (a) Fluctuation spectrum $F_q(s)$ as a function of s where $q = 2$, (b) Generalized Hurst exponent $h(q)$ as a function of q, and (c) Multifractal spectrum $f(\alpha)$ as a function of α of solar wind speed time series obtained using MFDFA1-4 during solar cycle 24.

Figure 4 shows the results that follow from this. Analysis of this figure shows that when one type of trend is retained in the profile or when fourth-order trends are eliminated, multifractality due to fat-tailed probability is the least dominant multifractality in the solar wind speed series during the study period. It is found

that the degree of multifractality of the surrogate data is lower than that of the original dataset. This shows that a broad, fat-tailed distribution would be the cause of multifractality in the solar wind speed time series during the study period. It is also observed that for any value of the order of the polynomial, $\Delta\alpha_{shuf} < \Delta\alpha_{surro} < \Delta\alpha$. This indicates that the strength of long-range correlation multifractality is lower than that of fat-tailed probability distribution multifractality. It follows that multifractality results from both a fat-tailed probability density function and long-range temporal correlations. The multifractal spectrum obtained is not symmetric. It has a long right tail, indicating that the contribution of small fluctuations is the most important. Moreover, whatever the order considered, the difference in the width of the spectrum between the original solar wind series and the shuffled series is higher than that found between the original solar wind series and the surrogated series. These results therefore show that the multifractal characteristics, the degree of multifractality and the origin of multifractality are strongly dependent on the type of detrending chosen.

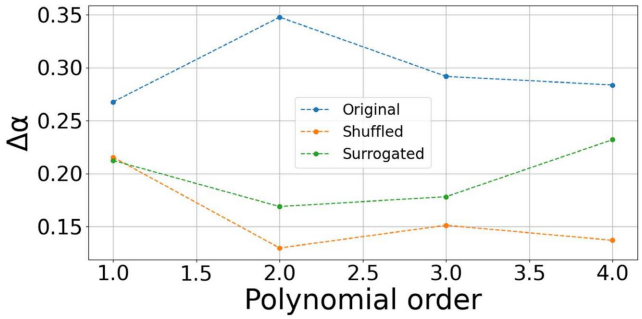

Figure 4. $\Delta\alpha - m$ plots of solar wind speed time series obtained using MFDFA1-4 (m = 1, 2, 3, 4) for original, shuffled, and surrogated data during solar cycle 24.

3.2. Interplanetary Magnetic Field

The interplanetary magnetic field plays a major role in the interactions between solar winds and the Earth's magnetosphere. **Figure 5** shows the temporal variation of its intensity during solar cycle 24. This figure shows that this parameter fluctuates significantly between 0.13 nT and 44.85 nT, with an average of 5.27 nT. During the minimum period of the solar cycle, the Sun's magnetic field resembles that of the Earth [39]. Based on the standard deviation values, the dynamics of the field appear to be more stable than that of the solar wind. We have plotted in **Figure 6** respectively the variation of the fluctuation spectrum (**Figure 6(a)**), the generalized $h(q)$ (**Figure 6(b)**) and the singularity spectrum function $f(\alpha)$ (**Figure 6(c)**), obtained using MFDFA1-4. In **Figure 6(a)**, the fluctuation spectrum $F(s)$ is plotted against s in a log-log diagram for the specific case where q = 2. Overall, the observed trend is the same for all values of order m. The fluctuation spectrum increases as the length of the segments increases. On the other hand, the fluctuations decrease when the order of the polynomial increases. This suggests multifractal behavior in this data set. The curve representing the generalized Hurst

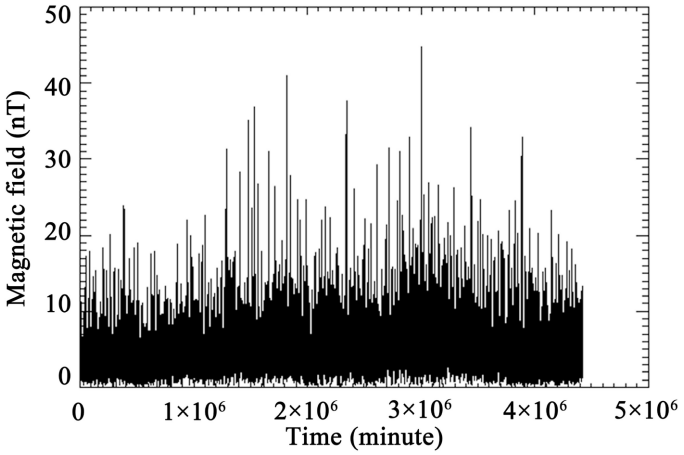

Figure 5. Variation of interplanetary magnetic field time series during solar cycle 24.

exponent is not constant (**Figure 6(b)**). It is noted that for any order of the polynomial, $h(q)$ decreases with increasing moment q. The curve for the first-order moment deviates widely from the curves of the others. Moreover, the dependence of the exponents $h(q)$ on q is less pronounced in the interplanetary magnetic field series, confirming the presence of long-range correlations and intermittency at several time scales. This evolution of $h(q)$ as a function of q indicates the existence of multifractal behavior in the magnetic field series during solar cycle 24. When the m^{th}-order trends (m = 1, 2, 3, 4) are eliminated from the profile, it is noted that the same exponent $h(q)$ varies little with increasing q, which shows weak multifractal behavior.

The curve representing the multifractal spectrum of the interplanetary magnetic field occur during solar cycle 24 also has the appearance of a concave function of α (**Figure 6(c)**). Globally, it is noted that the values of the Hölder exponent α are greater than 0.5 as what we got for wind speed. But for the moment of order 4, certain values of α are the exception. The width of this curve is an additional parameter witch can be identified as the degree of multifractality. Compared to what we obtained for the solar wind speed series, we notice that the width of the spectrum recorded here is less wide. This means that the probability distribution is less heterogeneous and therefore the degree of multifractality of the solar wind speed fields is high. The highest values of α are noted for m = 1. To better identify the origin of multifractality and assess the contribution of the two types of possible sources, we computed the corresponding multifractal spectrum width for the original series, shued series, and surrogated series.

Figure 7 shows the impact of shued and surrogated series on the initial multifractal spectrum width. For all polynomial orders, the $\Delta\alpha$ values for the substituted series are significantly lower than those for the shuffled series. This trend clearly indicates that the multifractality due to the fat-tailed probability is therefore the least dominant multifractality in our magnetic field data. Moreover, whatever the order of the polynomial considered, the curve of the width of the

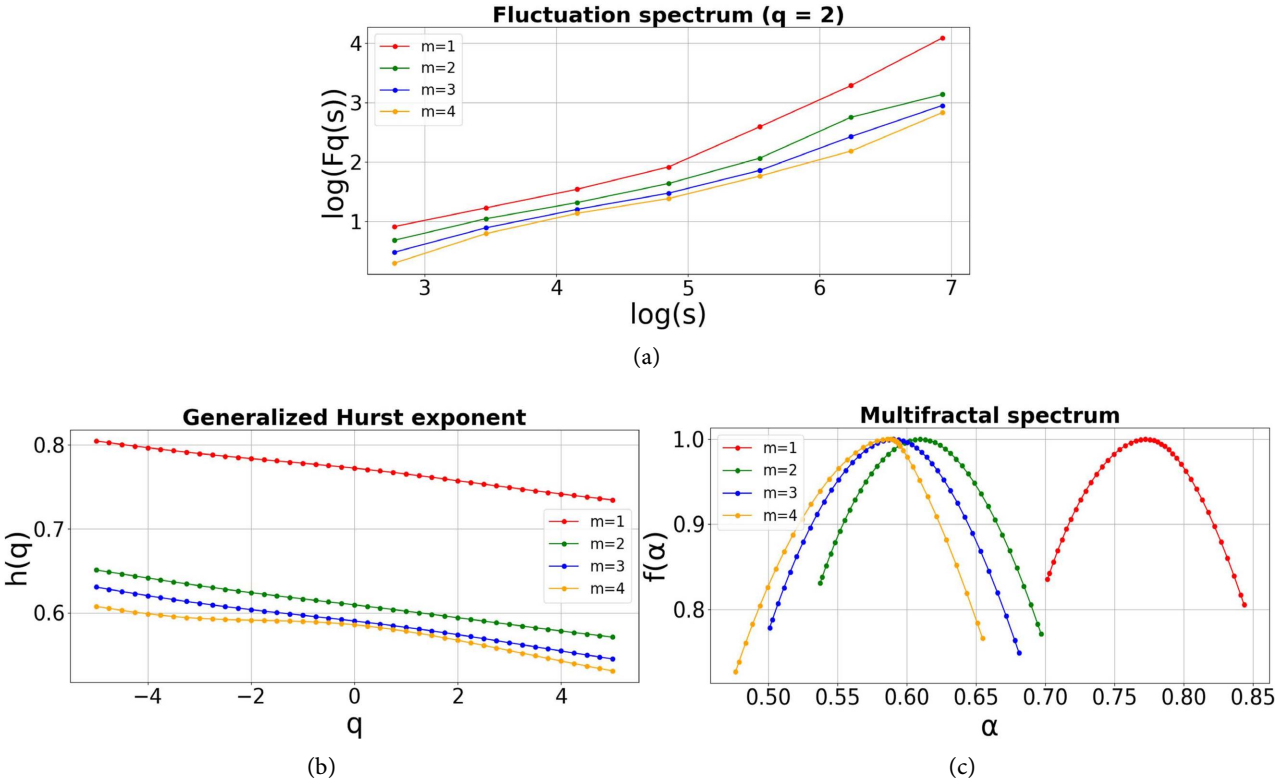

Figure 6. (a) Fluctuation spectrum $F(s)$ as a function of s where $q = 2$, (b) Generalized Hurst exponent $h(q)$ as a function of q, and (c) Multifractal spectrum $f(\alpha)$ vs. α of magnetic field intensity time series obtained using MFDFA1-4 during solar cycle 24.

spectrum of the shued series is clear below that surrogated, which reveals the presence of non-linearities in the series. We also note that for polynomials of order $m = 1$, $m = 2$ and $m = 4$, the values of the width of the initial multifractal spectrum and those shuffled are close. This indicates that multifractality comes mainly from the distribution of values. The difference recorded between these two widths for polynomial order m = 3 is quite significant.

Based on **Figure 3(c)** and **Figure 6(c)**, we have recorded in **Table 1** the numerical results of the representation of the singularity spectrum of both the solar wind speed and the interplanetary magnetic field. The maximum value reached by the function $f_{\max}(\alpha)$ is equal to 1, which is in perfect agreement with the schematic representation of **Figure 1**. This result, although compatible with several works, is however not in agreement with Sarkar *et al*'s [9] observations. Indeed, these authors have studied the nature of the fluctuation of the daily average solar wind speed time series collected over a period of 2492 days. They found that the maximum of the spectrum function is $f_{\max}(\alpha) = 2$. For all orders of polynomial tested, the maximum of values of $\Delta\alpha$ the multifractal spectrum witch is 0.35 obtained with solar wind speed. For both our data series, f is negative except for MFDFA4 for the magnetic field series, which induces a multi-scale fractal spectrum is shaped like a right hook.

Table 1. Numerical results extracted from the singularity spectrum of both **Figure 3(c)** and **Figure 6(c)**. To avoid confusion, parameter values relating to solar wind speed are written in italics.

Polynomial order		MFDFA1		MFDFA2		MFDFA3		MFDFA4	
Spectrum Parameter	$f_{max}(\alpha)$	*1*	1	*1*	1	*1*	1	*1*	1
	α_0	*0.735*	0.771	*0.687*	0.610	*0.728*	0.591	*0.745*	0.585
	$\Delta\alpha$	*0.274*	0.142	*0.350*	0.159	*0.278*	0.183	*0.276*	0.180
	Δf	*−0.325*	−0.027	*−0.15*	−0.058	*−0.1*	−0.027	*−0.045*	0.375

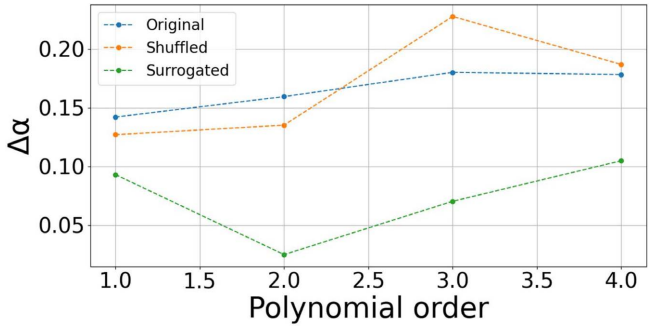

Figure 7. $\Delta\alpha - m$ plots of interplanetary magnetic field time series obtained using MFDFA1-4 (m = 1, 2, 3, 4) for original, shuffled, and surrogated data during solar cycle 24.

4. Conclusions

In this study, we analyzed both the fluctuations of the solar wind and the interplanetary magnetic field during solar cycle 24. We used high-frequency data of solar wind speed and interplanetary magnetic field strength over an eleven-year period from December 2008 to December 2019. This data is available and directly extracted from the NASA OMNIweb server database. The method used to analyze our two data sets is known as MFDFA (Multifractal Detrended Fluctuation Analysis) which is a powerful tool for identifying scaling behaviors and multifractal properties of nonstationary time series. We compared their degree of multifractality based on the evolution of the generalized Hurst exponents $h(q)$ and on the width of the singular spectrum $\Delta\alpha$.

The main results of this study have allowed us to improve our current knowledge on the complexity of the fluctuations behavior of the solar wind plasma velocity field as well as the interplanetary magnetic field during the cycle known to be the weakest cycle in terms of sunspots for several decades. It is clear from our investigation that the solar wind speed exhibits a more complex multifractal behavior than the interplanetary magnetic field. In other words, the internal structure of the solar wind speed appears to be governed by non-trivial scaling laws, reflecting a more marked fractal behavior. On the other hand, the intensity of the interplanetary magnetic field, by the relative narrowness of its spectrum, reveals a more homogeneous and less intermittent dynamic. The nature of the physical processes governing each of these quantities could be the cause of this difference.

Indeed, the dynamics of the solar wind is strongly marked by the coexistence of speed regimes (slow and fast), the presence of transient structures (coronal mass ejections, shock discontinuities, ...) and the development of compressible turbulence during expansion. These multiple contributions induce a hierarchy of temporal and spatial scales that can reinforce the fractal spectrum of the speed. On the other hand, the intensity of the interplanetary magnetic field is more constrained by the global topology imposed by the Parker spiral and by the conservation of magnetic flux during radial expansion. Its variations are often linked to Alfvenian waves and coherent structures, which could lead to a reduction in the diversity of multi-scale behaviors detectable in the interplanetary magnetic field intensity data set. It is also possible that the observed difference is linked to the use of scalar intensity which could mask part of the complexity contained in the vector components of the magnetic field. Furthermore, we noticed that the multifractality of the original series is caused partly by the large fat-tailed distribution of the original series or by nonlinear correlations, since the surrogate series exhibit lower multifractality than the original series. In view of the important results obtained at the end of this study, we will be interested in our future work in the Bz component of the interplanetary magnetic field by taking into account certain geomagnetic indices during the different phases (minimum, ascending, maximum and descending) of the solar cycle 24. Indeed, it has already been demonstrated in the literature that the intensity and orientation of the interplanetary magnetic field (particularly the B_z component) condition the coupling by magnetic reconnection which is often translated by geomagnetic indices. Based on this hypothesis, if the fractality of an index follows that of the interplanetary magnetic field rather than that of the speed, we will then be able to confirm that the magnetosphere responds more to magnetic fluctuations than to kinetic variations alone.

Acknowledgements

The authors thank two anonymous reviewers for their significant contributions to the success of this work.

Conflicts of Interest

The authors declare no conflicts of interest regarding the publication of this paper.

References

[1] Gomes, L.F., Gomes, T.F.P., Rempel, E.L. and Gama, S. (2022) Origin of Multifractality in Solar Wind Turbulence: The Role of Current Sheets. *Monthly Notices of the Royal Astronomical Society*, **519**, 3623-3634. https://doi.org/10.1093/mnras/stac3577

[2] Macek, W.M. (2007) Multifractality and Intermittency in the Solar Wind. *Nonlinear Processes in Geophysics*, **14**, 695-700.

[3] Salem, C., Mangeney, A., Bale, S.D. and Veltri, P. (2009) Solar Wind Magnetohydrodynamics Turbulence: Anomalous Scaling and Role of Intermittency. *The Astrophysical Journal*, **702**, 537-553. https://doi.org/10.1088/0004-637x/702/1/537

[4] Telesca, L., Lapenna, V., Vallianatos, F., Makris, J. and Saltas, V. (2004) Multifractal Features in Short-Term Time Dynamics of ULF Geomagnetic Field Measured in Crete, Greece. *Chaos, Solitons & Fractals*, **21**, 273-282. https://doi.org/10.1016/j.chaos.2003.10.020

[5] Mangeney, A. (2001) Summary of Session 1: Fundamental Processes in Space Physics from Macroscopic to Microscopic Scales. *Astrophysics and Space Science*, **277**, 117-122. https://doi.org/10.1023/a:1012236212752

[6] Podesta, J.J., Roberts, D.A. and Goldstein, M.L. (2006) Self-Similar Scaling of Magnetic Energy in the Inertial Range of Solar Wind Turbulence. *Journal of Geophysical Research: Space Physics*, **111**, 1-17. https://doi.org/10.1029/2006ja011766

[7] Bolzan, M.J.A. and Rosa, R.R. (2012) Multifractal Analysis of Interplanetary Magnetic Field Obtained during CME Events. *Annales Geophysicae*, **30**, 1107-1112. https://doi.org/10.5194/angeo-30-1107-2012

[8] Li, E., Mu, X., Zhao, G. and Gao, P. (2015) Multifractal Detrended Fluctuation Analysis of Streamflow in the Yellow River Basin, China. *Water*, **7**, 1670-1686. https://doi.org/10.3390/w7041670

[9] Sarkar, T., Khondekar, M.H. and Banerjee, S. (2001) Signal Processing Approach to Study Multifractality and Singularity of Solar Wind Speed Time Series. *International Journal of Computer and Information Engineering*, **11**, 168-173.

[10] Wawrzaszek, A. and Macek, W.M. (2010) Observation of the Multifractal Spectrum in Solar Wind Turbulence by Ulysses at High Latitudes. *Journal of Geophysical Research: Space Physics*, **115**, A07104. https://doi.org/10.1029/2009ja015176

[11] Agbazo, M., Koto N'Gobi, G., Adéchinan, A.J., Kounouhewa, B., Houngninou, B.E. and Afouda, A. (2020) Multifractal Characteristics of Cloud-To-Ground Lightning Intensity Observed in AMMA-CATCH Station (northern Benin). *Bulletin of Atmospheric Science and Technology*, **1**, 43-57. https://doi.org/10.1007/s42865-020-00004-7

[12] Shu, Z. and Chan, P.W. (2025) Application of Fractal Analysis on Wind Speed Time Series: A Review. *Advances in Wind Engineering*, **2**, Article ID: 100028. https://doi.org/10.1016/j.awe.2024.100028

[13] Krzyszczak, J., Baranowski, P., Zubik, M., Kazandjiev, V., Georgieva, V., Sławiński, C., et al. (2018) Multifractal Characterization and Comparison of Meteorological Time Series from Two Climatic Zones. *Theoretical and Applied Climatology*, **137**, 1811-1824. https://doi.org/10.1007/s00704-018-2705-0

[14] Lanzerotti, L.J. and Baker, D.N. (2017) Space Weather Research: Earth's Radiation Belts. *Space Weather*, **15**, 742-745. https://doi.org/10.1002/2017sw001654

[15] Alberti, T., Consolini, G., Carbone, V., Yordanova, E., Marcucci, M.F. and De Michelis, P. (2019) Multifractal and Chaotic Properties of Solar Wind at MHD and Kinetic Domains: An Empirical Mode Decomposition Approach. *Entropy*, **21**, Article 320. https://doi.org/10.3390/e21030320

[16] Consolini, G. and De Michelis, P. (2023) A Joint Multifractal Approach to Solar Wind Turbulence. *Fractal and Fractional*, **7**, Article 748. https://doi.org/10.3390/fractalfract7100748

[17] Macek, W.M., Bruno, R. and Consolini, G. (2006) Testing for Multifractality of the Slow Solar Wind. *Advances in Space Research*, **37**, 461-466. https://doi.org/10.1016/j.asr.2005.06.057

[18] Hnat, B., Chapman, S.C., Kiyani, K., Rowlands, G. and Watkins, N.W. (2007) On the Fractal Nature of the Magnetic Field Energy Density in the Solar Wind. *Geophysical*

Research Letters, **34**, L15108. https://doi.org/10.1029/2007gl029531

[19] de Figueiredo, B.C.L., Moreira, G.R., Stosic, B. and Stosic, T. (2014) Multifractal Analysis of Hourly Wind Speed Records in Petrolina, Northeast Brazil. *Revista Brasileira de Biometria*, **32**, 599-608.

[20] Bolzan, M.J.A., Rosa, R.R. and Sahai, Y. (2009) Multifractal Analysis of Low-Latitude Geomagnetic Fluctuations. *Annales Geophysicae*, **27**, 569-576. https://doi.org/10.5194/angeo-27-569-2009

[21] López-Lambraño, A.A., Fuentes, C., Serpa-Usta, Y., González Tejada, N.M. and López-Ramos, A. (2025) Multifractal Measures and Singularity Analysis of Rainfall Time Series in the Semi-Arid Central Mexican Plateau. *Atmosphere*, **16**, Article 639. https://doi.org/10.3390/atmos16060639

[22] Biswas, A., Zeleke, T.B. and Si, B.C. (2012) Multifractal Detrended Fluctuation Analysis in Examining Scaling Properties of the Spatial Patterns of Soil Water Storage. *Nonlinear Processes in Geophysics*, **19**, 227-238. https://doi.org/10.5194/npg-19-227-2012

[23] Zhang, L., Li, H., Liu, D., Fu, Q., Li, M., Faiz, M.A., et al. (2021) Application of an Improved Multifractal Detrended Fluctuation Analysis Approach for Estimation of the Complexity of Daily Precipitation. *International Journal of Climatology*, **41**, 4653-4671. https://doi.org/10.1002/joc.7092

[24] Dutta, S., Ghosh, D. and Chatterjee, S. (2013) Multifractal Detrended Fluctuation Analysis of Human Gait Diseases. *Frontiers in Physiology*, **4**, Article 274. https://doi.org/10.3389/fphys.2013.00274

[25] Adarsh, S., Nityanjaly, L.J., Pham, Q.B., Sarang, R., Ali, M. and Nandhineekrishna, P. (2021) Multifractal Characterization and Cross Correlations of Reference Evapotranspiration Time Series of India. *The European Physical Journal Special Topics*, **230**, 3845-3859. https://doi.org/10.1140/epjs/s11734-021-00325-4

[26] Xia, D., Yu, W., Lin, L., Lin, X. and Hu, Y. (2025) Fractal Characteristics of Wind Speed Time Series Under Typhoon Climate in Southeastern China. *Fractal Fract.*, **9**, 175. https://doi.org/10.3390/fractalfract9030175

[27] Devi, R.R. and Chattopadhyay, S. (2024) Multifractal Detrended Fluctuation Analysis Approach to the Monthly Total Ozone Concentration over New Delhi, India. *Indian Journal of Physics*, **98**, 4635-4641. https://doi.org/10.1007/s12648-024-03204-5

[28] Zhan, C., Liang, C., Zhao, L., Zhang, Y., Cheng, L., Jiang, S., et al. (2021) Multifractal Characteristics Analysis of Daily Reference Evapotranspiration in Different Climate Zones of China. *Physica A*: *Statistical Mechanics and its Applications*, **583**, Article ID: 126273. https://doi.org/10.1016/j.physa.2021.126273

[29] Stosic, B., Stosic, T., Tošić, I. and Djurdjević, V. (2025) Multifractal Analysis of Temperature in Europe: Climate Change Effect. *Chaos, Solitons & Fractals*, **196**, Article ID: 116386. https://doi.org/10.1016/j.chaos.2025.116386

[30] Gómez-Gómez, J., Plocoste, T., Alexis, E., Jiménez-Hornero, F.J., Gutiérrez de Ravé, E. and Nuiro, S.P. (2023) Multifractal Detrended Fluctuation Analysis of Rainfall Time Series in the Guadeloupe Archipelago. *Journal of Hydrology*, **626**, Article ID: 130377. https://doi.org/10.1016/j.jhydrol.2023.130377

[31] Peng, C.-., Buldyrev, S.V., Havlin, S., Simons, M., Stanley, H.E. and Goldberger, A.L. (1994) Mosaic Organization of DNA Nucleotides. *Physical Review E*, **49**, 1685-1689. https://doi.org/10.1103/physreve.49.1685

[32] Kantelhardt, J.W., Zschiegner, S.A., Koscielny-Bunde, E., Havlin, S., Bunde, A. and Stanley, H.E. (2002) Multifractal Detrended Fluctuation Analysis of Nonstationary

Time Series. *Physica A*: *Statistical Mechanics and Its Applications*, **316**, 87-114. https://doi.org/10.1016/s0378-4371(02)01383-3

[33] Tokpanoudé, J.D., Adéchinan, J.A. and Kpomahou, F.Y.D. (2025) Fractal Dimension of Solar Wind Speed at Different Time Scales Using Box Counting Method. *Physical Science International Journal*, **29**, 1-11. https://doi.org/10.9734/psij/2025/v29i2873

[34] Movahed, M.S., Jafari, G.R., Ghasemi, F., Rahvar, S. and Tabar, M.R.R. (2006) Multifractal Detrended Fluctuation Analysis of Sunspot Time Series. *Journal of Statistical Mechanics*: *Theory and Experiment*, **2006**, P02003. https://doi.org/10.1088/1742-5468/2006/02/p02003

[35] Bhoumik, G., Deb, A., Bhattacharyya, S. and Ghosh, D. (2016) Comparative Multifractal Detrended Fluctuation Analysis of Heavy Ion Interactions at a Few GeV to a Few Hundred GeV. *Advances in High Energy Physics*, **2016**, Article ID: 7287803. https://doi.org/10.1155/2016/7287803

[36] Rydin Gorjão, L., Hassan, G., Kurths, J. and Witthaut, D. (2022) MFDFA: Efficient Multifractal Detrended Fluctuation Analysis in Python. *Computer Physics Communications*, **273**, Article ID: 108254. https://doi.org/10.1016/j.cpc.2021.108254

[37] Kwapień, J., Oświe¸cimka, P. and Drożdż, S. (2005) Components of Multifractality in High-Frequency Stock Returns. *Physica A*: *Statistical Mechanics and Its Applications*, **350**, 466-474. https://doi.org/10.1016/j.physa.2004.11.019

[38] Yu, M., Xing, L., Wang, L., Zhang, F., Xing, X. and Li, C. (2023) An Improved Multifractal Detrended Fluctuation Analysis Method for Estimating the Dynamic Complexity of Electrical Conductivity of Karst Springs. *Journal of Hydroinformatics*, **25**, 174-190. https://doi.org/10.2166/hydro.2023.043

[39] Dong, Q., Wang, Y. and Li, P. (2017) Multifractal Behavior of an Air Pollutant Time Series and the Relevance to the Predictability. *Environmental Pollution*, **222**, 444-457. https://doi.org/10.1016/j.envpol.2016.11.090